Journal of Physics:
Conference Series

PAPER • **OPEN ACCESS**

The global blockage effect of a wind farm cluster - an LES study

To cite this article: J Meijer *et al* 2024 *J. Phys.: Conf. Ser.* **2767** 092093

Journal of Physics: Conference Series **2767** (2024) 092093 doi:10.1088/1742-6596/2767/9/092093

The global blockage effect of a wind farm cluster - an LES study

J Meijer[1,2], G Steinfeld[1,2], L Vollmer[3], and M Dörenkämper[3]

[1] Carl von Ossietzky Universität Oldenburg, School of Mathematics and Science, Institute of Physics
[2] ForWind - Center for Wind Energy Research, Küpkersweg 70, 26129 Oldenburg, Germany
[3] Fraunhofer Institute for Wind Energy Systems (IWES), Küpkersweg 70, 26129 Oldenburg

E-mail: jorrit.meijer@uni-oldenburg.de

Abstract. The interaction of wind farm clusters with the atmospheric flow is complex. It comes along with phenomena that have still not been fully understood in detail. However, having an understanding of the flow is a prerequisite for the derivation of models that can accurately and with limited computational resources replicate the most prominent features of the flow. This study exploits large-eddy simulations (LES) to create a better understanding of the wind farm cluster blockage under a set of different atmospheric conditions. The specific wind farm cluster consists of three wind farms, with a relatively narrow gap between the two northernmost wind farms. Results reveal that under conventionally neutral boundary layers, the induction zone relatively large is when there is a low atmospheric boundary layer height with a strong temperature inversion. In our LES study, wind speed is reduced between 2 % and 4 % 2 D upstream of the front row of the wind farm, while inside the gap of the wind farm cluster, there is an acceleration of the wind speed. Comparatively, blockage for a solitary row or single wind turbine is similar and smaller than for a whole cluster. On average, turbines in the front row of a cluster produce 5.1 % less power than a single turbine.

1. Introduction

The utilization of renewable energies is growing globally. However, being dependent on changes in weather, renewable energies have their own inherent threats. Moreover, extending the utilization of renewable energies come along with challenges. Namely, the maximization of power output for large wind farms, which is one of the leading factors for wind farm designers and operators. The power output of wind farms is known to be affected by interactions between the wind turbines. Currently, the largest share of power loss in a wind farm is attributed to wake losses, as turbines in the wake of another turbine receive less kinetic energy.

Recent investigations indicate that in simple terrain, such as offshore wind farms, the installation of numerous turbines not only locally obstructs the flow but collectively causes a larger-scale reduction in wind speed upstream, termed 'global blockage' [1]. Previously (i.e. *Allaerts & Meyers [2]*) found a global blockage effect in large-eddy simulations (LES) of semi-infinite wind farms, connecting the phenomena to the stratification of the atmospheric boundary layer (ABL). *Abkar & Porté-Agel* [3] investigated the impact of the strength of the capping inversion on the flow conditions in and around very large wind farms, claiming that a stronger capping inversion leads to a decrease of the total power produced by the wind farm. *Wu &*

Porté-Agel [4] pointed out by an LES study that under a conventionally neutral atmospheric boundary layer (CNBL), the extent of the induction zone is dependent on the strength of the stratification in the ABL, where a stronger stratification leads to a greater induction that is also larger in space.

Not only has the blockage effect been studied by numerical simulations, but also field observations have been conducted. *Bleeg et al.* [1] were one of the first to observe large induction zones (extending at least up to 7 D) upstream of a wind farm with met mast observation data. Their findings revealed a 1.9 % reduction in wind speed 7 D to 10 D upstream at hub height. *Schneemann et al.* [5] experimentally investigated the induction effects on a 400 MW offshore wind farm with a lidar scanning the flow at the height of the transition piece (25 m) of the wind turbine, showing that in a stably stratified atmosphere, a velocity deficit upstream of the turbine is measurable at that height.

More recently, *Maas & Raasch* [6] studied the wake properties and power production under different atmospheric conditions for the entire German Bight by LES, assuming further exploitation of wind resources, highlighting that under mainly shallow, stable boundary layers there is a significant global blockage occuring.

For this study we use the wind farm cluster N4. It is situated in the German Bight 30 km north of the island of Heligoland. The cluster is simulated in its state before 2023. Therefore, the cluster consists out of three wind farms. Between the two northernmost wind farms there is a zone free of wind turbines. This zone has a width of 3.5 km. Even though there are already studies conducted on the N4 cluster [7], the flow conditions in the gap have not yet been studied in detail before.

Whereas many LES studies, such as the ones previously mentioned, explored exclusively wind farms with idealized layouts, or with assumed future wind farm exploitations, this study explores an isolated operational wind farm cluster equipped with different turbines. We exclusively study the effect of conventionally neutral atmospheric boundary layers, since they occur frequently over sea. Therefore, we would like to answer what the dependency of the global blockage effect is on the height and strength of the inversion layer. We want to exclude that solely the ABL height has an influence by also simulating different strengths of the capping inversion at the same height. Moreover, we want to answer what the impact of global blockage has on the front row of the wind farm cluster, and whether we see differences with a solitary row or a single turbine. This also allows us to quantify the power loss of the front row, highlighting the difference between single turbine induction and global blockage.

The structure of the paper is as follows: In Section 2, we introduce the methodology and domain setup, including the initial conditions. Section 3 contains the results, divided into two parts. The first part compares the outcomes of our LES model under various stratifications inside the temperature inversion and varying height of the ABL, while the second part of the section contrasts the strongest global blockage case for the entire cluster with a single row and a single turbine setup. The discussion takes place in Section 4. Finally, Section 5 concludes our findings and suggests directions for extending this study.

2. Numerical framework

The following section introduces the LES code "Parallelized Large-eddy Simulation Model" (PALM). We elaborate on the Actuator Disk Model (ADM) , and domain setup for precursor and main simulations.

2.1. Model description

The LES code PALM has been used in this study. The model employs the non-hydrostatic, filterered, incompressible Navier-Stokes equations with Boussinesq approximation. Further details about PALM can be found in [9].

The wind turbine modeling is done by employing an ADM approach [10]. This only requires the rotor diameter, hub height, and C_T-curves to be given to the model. The turbines in the modeled domain exert a drag force f_T on the flow:

$$f_T = \frac{F}{A} = \frac{1}{2}\rho_0 u_\infty^2 C_T \tag{1}$$

where u_∞ is the reference velocity at hub height, commonly known as the free-stream velocity, and C_T is the thrust coefficient. This C_T parameter is typically provided in a table in dependency from the upstream (free-stream u_∞) wind speed. The reference velocity u_∞ is a crucial parameter since it depicts the local induction caused by the stand alone turbine. To approximate the free stream in the current timestep t ($u_{\infty,t}$), we take the actual induction a factor from the previous time iteration (a_{t-1}), such that:

$$u_{\infty,t} = v_{\text{eq}} \left(\frac{1}{1 - a_{t-1}} \right) \quad \text{with} \quad v_{\text{eq}} = \left(\sum_{i=1}^{n_h} \left(v_i \cos\left(|\chi_i - \chi_{HH}| \right) \right)^3 \frac{A_i}{A} \right)^{\frac{1}{3}} \tag{2}$$

with the total number of chosen height sections n_h, the average wind speed and direction in the i-th height segment v_i and χ_i, the hub height wind direction χ_{HH}, the area of the i-th segment A_i, and the total rotor swept area A. The axial induction factor a is computed as:

$$a = \frac{1}{2} \left(1 - \sqrt{1 - C_T(u_\infty)} \right) \tag{3}$$

The ADM assumes a constant density of $\rho_0 = 1.225\,\text{kgm}^{-3}$. The power of the turbines are determined by estimating the power coefficient C_P, which is derived by the axial induction factor a, obtained by the C_T of the free-stream's rotor equivalent wind speed, such that:

$$P = \frac{1}{2}\rho_0 C_P v_{\text{eq}}^3 A \quad \text{with} \quad C_P = 4a\left(1 - a\right)^2 . \tag{4}$$

To maintain steady turbulent inflow conditions, we apply the use of a turbulence recycling method. This method involves a precursor run and a main run. The inflow conditions are obtained by combining the mean profiles of the precursor run with the turbulence signal obtained in the recycling plane. The positioning of the recycling plane can be seen in Figure 1. Further details of the recycling method are given in *Maas & Raasch* [6].

2.2. Precursor run

For each of the case studies it is necessary to carry out a so-called precursor run, followed by the main run. The precursor run generates a quasi-stationary turbulent flow that can then be mapped to the domain of the main run. This ensures a well developed flow and reduces the domain flow-throughs required until the condition of a quasi steady state is reached in the main run. For this particular study, the domain of the precursor run is 750 times smaller than the one of the main run. Table 1 shows the boundary conditions for the precursor domain. We prescribe different initial starting values of the boundary layer heights ($\updownarrow h$), to eventually reach the desired ABL height. Since the ABL growths infinitely due to mechanical shear.

Not shown in Table 1 are the parameters of the Coriolis force, which is dependent on the latitudinal position. This we have set to 54°, approximately the position of the wind farm cluster. The resulting Coriolis frequency is $f = 10^{-4} s^{-1}$. The names of the cases describe the height of the capping inversion with their respective strength, i.e. CNBL-400-1 describes a set-up in which the height of the inversion layer is 400 m and the potential temperature gradient in the inversion layer is 1 K/100 m. The roughness length z_0 is set at 0.0002 m.

Case	$\updownarrow h$ $[m]$	u_g $[ms^{-1}]$	v_g $[ms^{-1}]$	G $[ms^{-1}]$	α $[\circ]$	$\updownarrow$ I $[m]$	θ $[K/100m]$	duration $[h]$
CNBL-400-1	300	9.96	-2.19	10.20	12.12	80	1.00	25.0
CNBL-400-03	10	10.03	-1.82	10.20	10.11	80	0.30	34.7
CNBL-800-1	750	10.06	-1.44	10.16	8.06	60	1.00	50.0
CNBL-800-03	670	10.09	-1.46	10.20	8.14	60	0.30	50.0

Table 1: Overview of the precursor run initial settings with boundary layer height h, geostrophic wind components u_g and v_g, G being the absolute geostrophic wind vector, geostrophic wind direction α, I the temperature inversion height, potential temperature gradient above ABL Θ, and duration of the precursor run h.

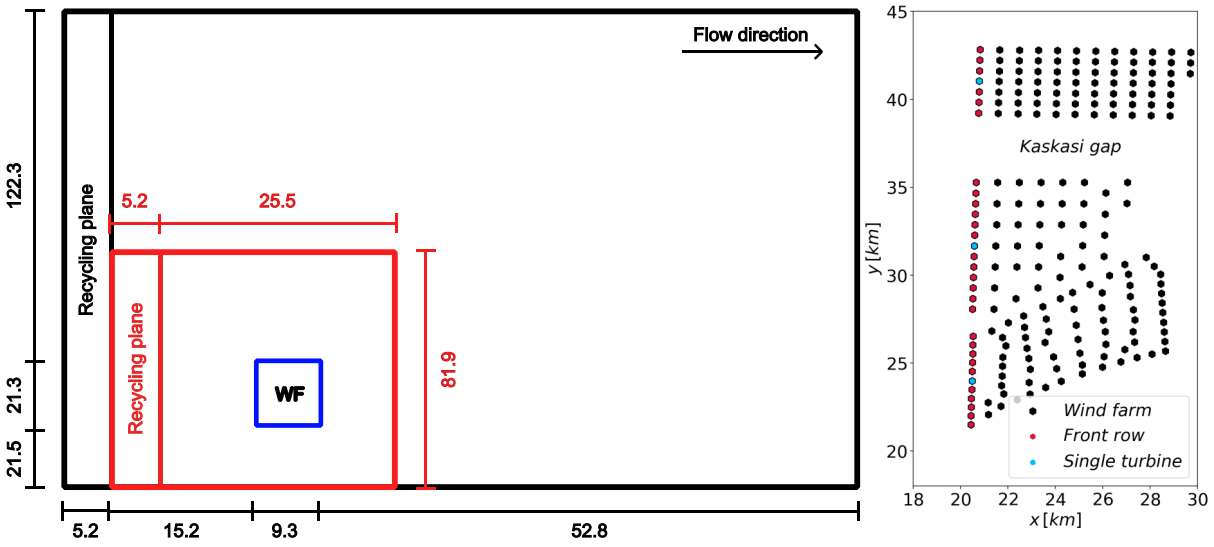

Figure 1: Left: Sketch of the domain setup with their relative location for the wind farm cluster (black dimensions), and solitary row and single turbine (red dimensions). Right : Wind farm cluster layout (black), and the respective chosen turbines: solitary row (red) and single turbine (blue)

2.3. Main run

The wind farm layout and its domain are based on the positions seen in Figure 1 (left). The length of the wind farm cluster (black in Figure 1 (left)) domain is $L_x = 82.6\,\text{km}$ and the width is $L_y = 165.1\,\text{km}$. The number of points in the x-direction is $n_x = 4128$ and in y-direction it is $n_y = 8256$. In both dimensions a grid spacing of $\Delta x = \Delta y = 20\,\text{m}$ is used. The z-direction has a grid spacing of $\Delta z = 10\,\text{m}$ up to 1000 m. Above this height it is stretched vertically with a stretching factor of $dz = 1.08$, whereas the maximum stretching is reached when $\Delta z_{max} = 50\,\text{m}$. This altogether manifests in a total domain height of 6.8 km. We intentionally apply a Rayleigh damping at 1000 m to prevent gravity wave interference. The strength of this Rayleigh damping is $f_{rd} = 0.01$.

In order to reduce the computational time required, the domain for the single row and single turbine cases has been shortened. Figure 1 (left) shows the shortened domain in red. The length of this domain is $L_x = 30.7\,\text{km}$ along the x-direction and $L_y = 81.9\,\text{km}$ along the y-direction. As a result, the single row and single turbine were also moved closer (5 km) to the recycling plane. The number of cells in x-direction is $n_x = 1535$ and y-direction is $n_y = 4095$. Other boundary conditions such as Rayleigh damping and height of the domain remain identical for

all simulations independent from the number of wind turbines simulated in it.

Within the wind farm cluster reside three different types of wind turbines. The hub heights of these turbines range from 89 m to 96 m, with a rotor diameter of 120 m to 126 m respectively. The turbines have an approximate spacing of 4 D to 5 D.

3. Results

In this section, we initially outline and analyze the observations of the wind farm cluster across different atmospheric conditions. Subsequently, we undertake a comparative analysis, focusing on that of our cases in which the blockage effect is most pronounced with the first row of the cluster (now referred to as solitary row) and a single turbine. All results shown in this section are averaged to the last 1.5 h of the simulation for the wind farm, and 2.5 h for the solitary row and single turbine.

3.1. Atmospheric variability and wind farm clusters

We present results from the simulations of four different atmospheric boundary-layers, as mentioned in Table 1. Figure 2 shows the horizontal wind speed, normalized by the free-stream wind speed u_∞, averaged across the y-axis from the southernmost to the northernmost wind turbine of the wind farm cluster. Across all scenarios, a zone with reduced wind speeds, whether minimal or extensive, is observable upstream of the wind farm cluster. The results shown in Figure 2b provide compelling evidence that the intensity of the capping inversion significantly influences the blockage in front of the wind farm. This observation is evident in both the CNBL-400 and CNBL-800 cases, where a stronger temperature inversion has more of a reduction of the wind speed upstream. The contrast in blockage is greater at the CNBL-400 cases, whereas the CNBL-800 cases have minor differences.

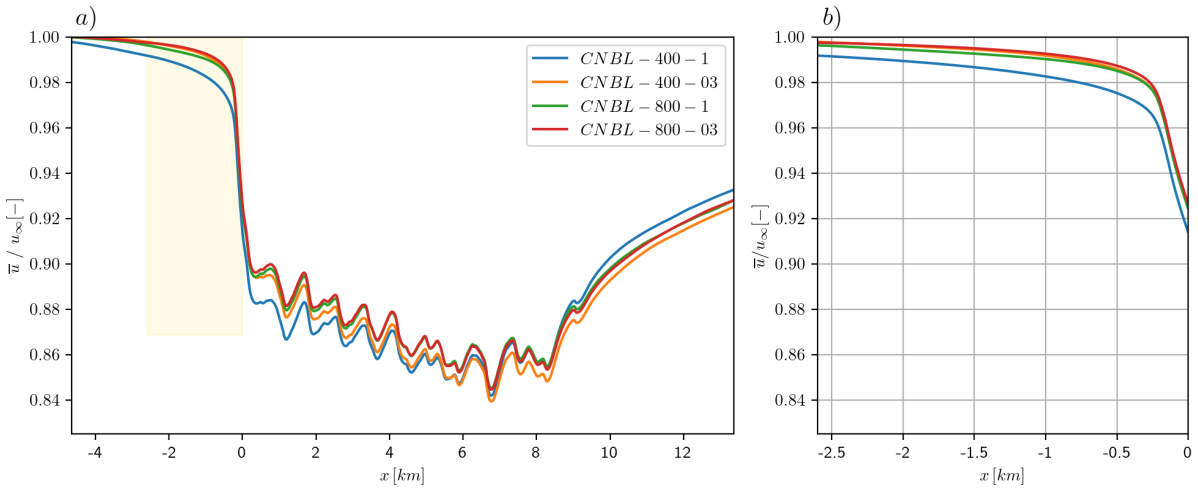

Figure 2: Time-averaged streamwise velocity at hub height normalised by the free stream velocity at hub height averaged over the entire wind farm cluster in the span-wise direction, including the Kaskasi gap (a). (b) Shows a zoom into the golden area seen in (a).

We observe a significant extension of the induction zone, especially for CNBL-400-1, reaching approximately 4 km upstream. Upon closer examination, except for CNBL-400-1, the cases follow relatively similar characteristics, with CNBL-800-1 showing a slightly greater reduction in wind speed at all distances. For example, at a distance of 800 m upstream (approximately 7 D), the flow velocity has diminished by 2 %, a seemingly modest percentage.

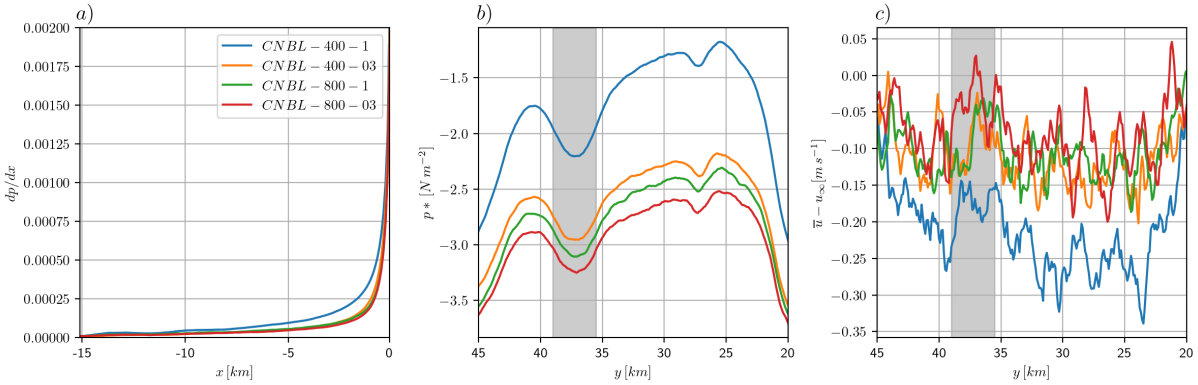

Figure 3: Upstream pressure perturbation gradient at hub height averaged in y-direction for the entire wind farm cluster (a), pressure perturbation along the y-axis averaged between 0 D to 8 D upstream of the wind farm cluster (b), and the wind speed deficit along the y-axis averaged between 0 D to 8 D upstream of the wind farm cluster (c). The grayed area in (b) and (c) represent the Kaskasi gap.

We can attribute the increased induction observed in the CNBL-400-1 case to a more pronounced pressure gradient upstream, distinguishing it from the other simulations. Figure 3a shows the pressure perturbation gradient in x-direction at hub height, position $x = 0$ states the first row of the cluster. The perturbation pressure is greatest right in front of the wind farm cluster, where CNBL-400-1 exhibits the largest perturbation pressure gradient. This can also be seen in Figure 3b. Here we show the absolute perturbation pressure along the spanwise direction of the wind farm cluster, averaged between 0 and 8 D upstream. Each case shows similar characteristics, such as an increase in perturbation pressure close to the center of the wind farm. And a decrease in perturbation pressure in the Kaskasi gap. The pressure along the y-direction shows an acceleration of the flow towards the Kaskasi gap, this creates a convergence of the v-component that must be compensated by a a divergence in the u-component (Figure 3c). For all four cases, the Kaskasi gap causes a relative speed up, this can be observed in the gray region.

Figure 4 is presented to provide a clearer representation of the actual global blockage induction zone, depicted in blue. In the interest of brevity, only two out of the four cases are shown. We observe that the blockage effect not only extends further upstream, but is also stronger in the CNBL-400-1 scenario. Further, two noteworthy observations emerge from this analysis. First, the blockage effect reaches into the Kaskasi gap, and second, it accelerates throughout space, surpassing even the freestream velocity. This phenomenon is consistently observed across all simulated cases. To gain a more insightful perspective on the horizontal wind speed component, specific positions within the Kaskasi gap are examined.

These designated positions, denoted as (A), (B), (C), and (D) in Figure 4, correspond to specific locations highlighted in Figure 5. Here we observe that the flow is not only affected in front of the wind farm cluster but is also obstructed within the Kaskasi gap, specifically along the centerline of the front row ($x = 0$) up to a distance of 4 km inside the gap. When we look further into the gap (8 km to 12 km), we notice an acceleration of the flow, exceeding the freestream velocity.

The speed-up in the Kaskasi gap, between the downstream wakes, remains persistent until the end of our domain (not shown). Additionally, we observe two other phenomena. First, an acceleration of the flow at about the height of the temperature inversion. This streamwise acceleration is related to a convergence of the flow in vertical direction at that height leading to

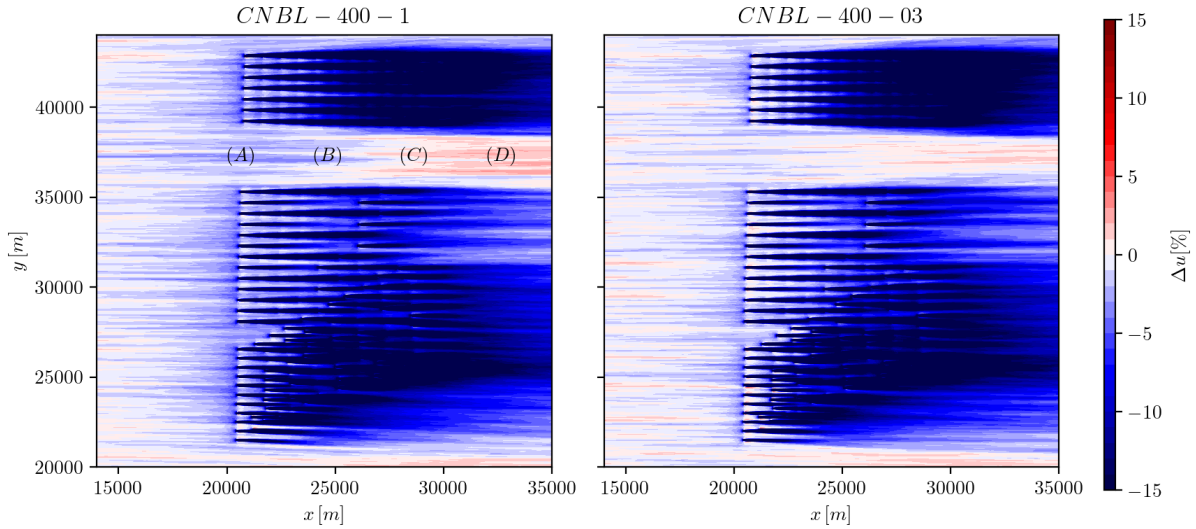

Figure 4: Time-averaged hub-height wind speed deviation normalised from the inflow of Heligoland wind farm cluster for different strengths of the capping inversion.

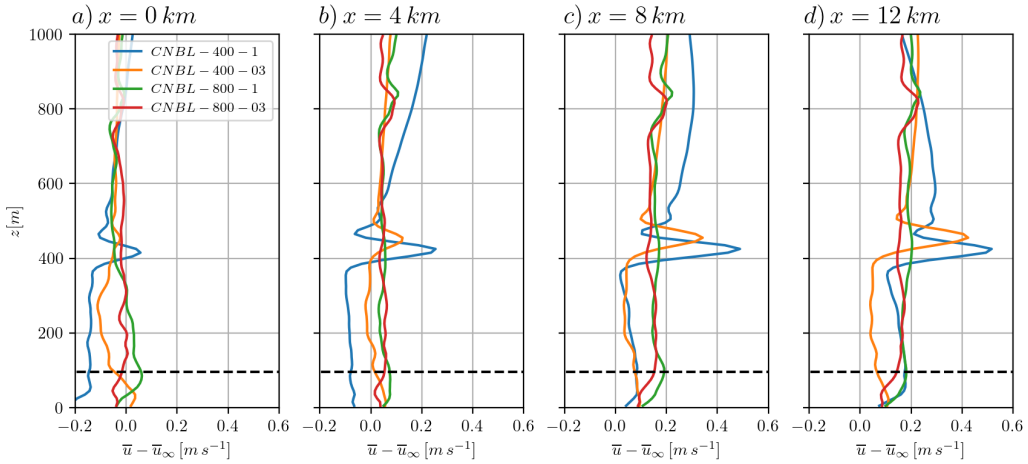

Figure 5: Time-averaged horizontal wind speed deviation normalised from the inflow of Heligoland wind farm cluster for different strength of the capping inversion inside the Kaskasi gap. (a) - (d) Represent the positions at which the horizontal profiles are being observed.

a divergence i.e. an acceleration of the flow in the x-direction. And secondly, a speed-up in the free atmosphere (most likely also due to the convergence of the flow in vertical direction).

3.2. Front row blockage: wind farm cluster, solitary row and single turbine

Here we take a closer look at the particular case that showed the strongest reduction of the wind speed and compare it with a solitary row of turbines and a single wind turbine.

Important to note is that the solitary row and single turbine domain is moved 5 km closer to the inflow. This does not impact the solution however, since prior empty-box simulations do not show a spatial development of the flow.

Figure 6 illustrates the velocity deficit upstream of a standalone turbine, solitary row, and wind farm cluster. Specifically, they depict the time-averaged streamwise velocity deficit at

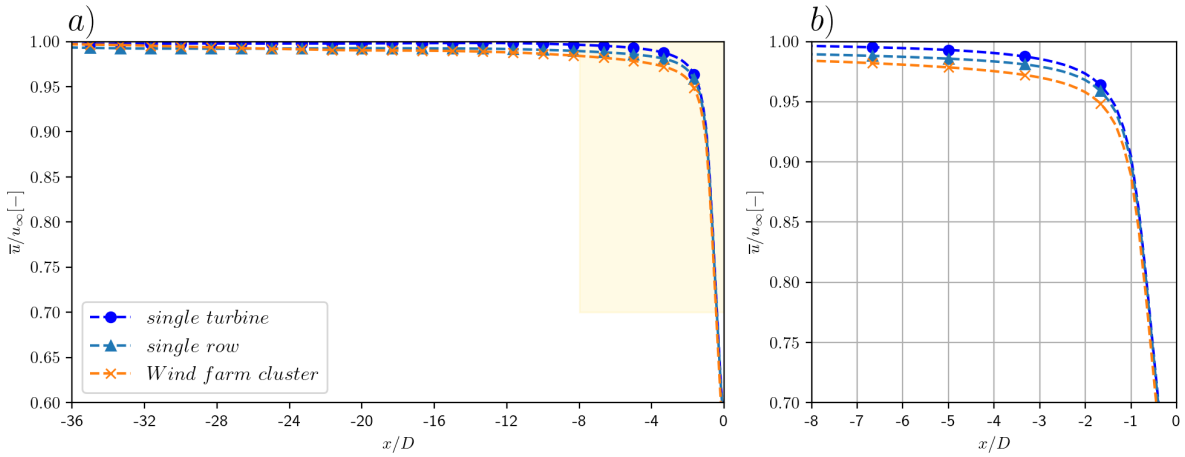

Figure 6: The normalized streamwise velocity, time-averaged and measured at hub height along the centerline upstream of each of the three turbines: isolated, solitary row, and wind farm, at the position of the northern isolated wind turbine. The figure on the right hand side shows a zoom into the region, depicted in gold (left).

hub height along the turbine's centerline, normalized by the free stream velocity. We observe that the single turbine is outperforming the other cases beyond 2 D upstream, whereas it has a similar induction behaviour as the solitary row at 2 D or closer. As for the solitary row, we can see that the induction on average is more pronounced than that of the single turbine. This exhibits mainly to the extent of the induction zone upstream. For instance, we observe a flow deceleration of 0.6 % between 16 D and 12 D upstream of the wind turbine. In other studies (such as [8]), they observed a 0.1 % deficit at 12 D for close turbine spacing (1.26 D).

We see, however, less of a overall reduction in the solitary row of turbines for the other cases compared to *Strickland et al.* [8]. One reason is that we do not apply an infinite row of turbines, allowing the flow to bypass the solitary row on the sides, and we have a relatively favourable turbine spacing (4 D to 5 D).

3.3. Front row power production: wind farm cluster, solitary row and single turbine

As for the power production, we only consider front row power production since due to inhomogeneous turbine spacing, it is impossible to distinguish downstream rows with one another inside the wind farm cluster. Since the power is normalized around the stand-alone turbine, we observe a 100 % efficiency for these turbines, as seen in Figure 7c. The data indicates that the front row of the wind farm cluster generates 5.1 % less power than a single turbine. However, interestingly, the average power produced by the solitary row is higher than that of a standalone turbine. On average, if we take the mean of the row, there is 0.5% more power produced.

4. Discussion

The LES cases are assessed for the existence of the global blockage effect. We compared four different sets of conditions under a conventionally neutral boundary layer, where we observed the occurrence of global blockage for each separate case, in which blockage was most dominantly present at low ABL heights (400 m) with a strong temperature inversion ($\Gamma = 1\,K/100\,m$). For this particular case, we observed an induction of 4 % at 5 D upstream and 2 % at 10 D. Consistent findings are evident in related studies. For example, *Bleeg et al* [1] noted a deficit of 1.9 % approximately 7 D to 10 D upstream, mirroring our observations. *Strickland et al*

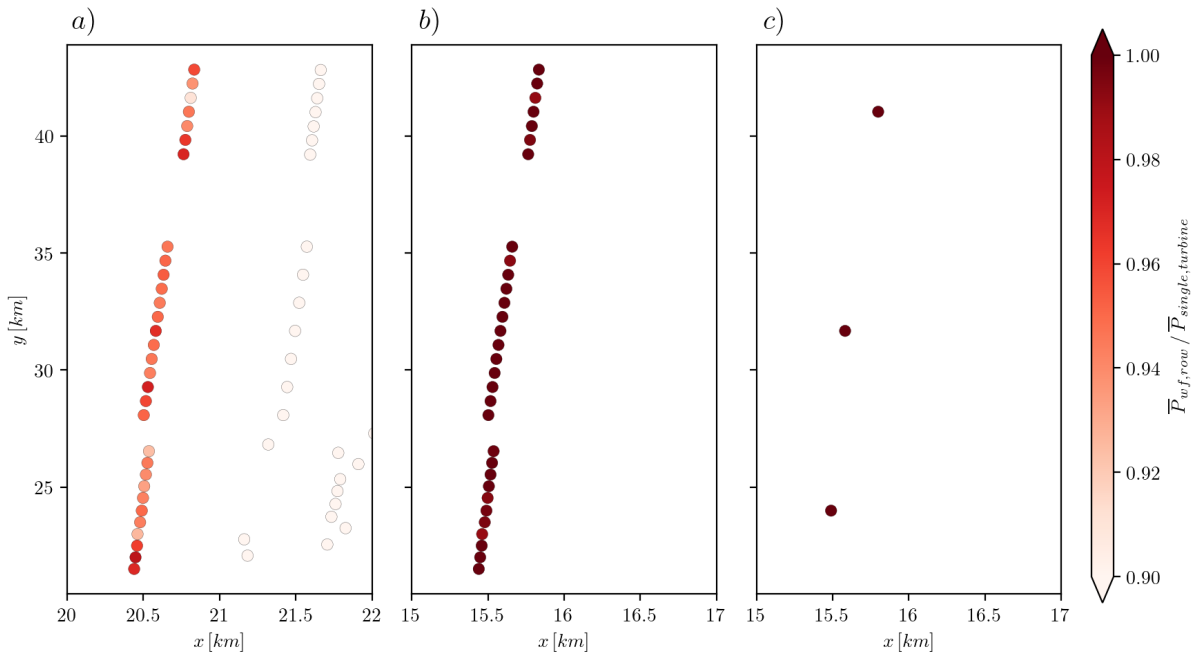

Figure 7: Wind turbine power production for the wind farm cluster (a), single front row (b), and single turbine (c). The power production is normalized around the single turbine (c).

[8] similarly reported comparable outcomes in a neutral ABL under varying turbine spacing conditions.

The presence of the wind farm cluster causes the flow to deflect, causing vertical advection of horizontal momentum, and creating a perturbation pressure gradient upstream of the wind farm cluster. Similar findings are observed in *Gomez et al.* [12]. We can also link the advection of momentum to the accelerations inside the Kaskasi gap. Caused, firstly, by a net momentum transport from the sides that accelerates the flow inside the gap. And secondly, the wind farm cluster necessitates that pressure returns to ambient levels downstream. As a result, it creates a pressure gradient from the front to the back, which in turn accelerates the flow within the gap. This speed up remains consistent throughout long distances, reaching the end of the domain (60 km downstream of the wind farm cluster). Similar findings were reported by *Maas* [11] in simulations of a large-scale wind farm, showing flow accelerations at the sides of the wind farm.

Not only does the flow accelerate inside the Kaskasi gap, but it also accelerates above the ABL. Our presumption is that the wind farm induces inertial gravity waves in the free atmosphere, leading to speed variations. While it is crucial to acknowledge that although other studies (e.g., *Smith et al.* [13] and *Lanzilao & Meyers* [14]) propose a connection between inversion layer displacement, pressure perturbations, and gravity wave excitations, this is beyond the current study's scope and warrants further exploration in subsequent research stages.

We also compared the case with the strongest blockage effect with a solitary row and single turbine under the same atmospheric conditions. This shows that for the close regions (2 D and closer) the solitary row and single turbine's induction is similar, whereas the wind farm cluster remains to have the most reduced upstream deficits. This is also shown in the front row power production, where the wind farm cluster produced 5.1 % less power compared to the single turbine. This is mainly due to the hindrance of downstream turbines, where the wind flow diverges over and around the wind farm, rather than going through it. The solitary row to the contrary produced 0.5 % more power.

This solitary row power increase is most likely due to the enhancement of blockage for the front row power production, where the flow is directed into the rotor-swept area of neighbouring turbines rather than deflecting around the turbine, whereas this effect will most likely increase the power production even more when spacing the turbines even closer to each other.

Previous studies, e.g. *Meyer Forsting et al.* [15] showed with RANS that when the turbines are positioned in a staggered pattern with a distance of 3 D, that there is a 0.57 % power production increase. In more recent work, *Strickland et al.* [8] also found within LES that there is more power being produced in an infinite row of wind turbines, compared to a stand-alone turbine. The discussion whether a solitary row can produce more than a single turbine is discussed in the work of *Bleeg & Montavon* [16]. They discuss the limitations of *Meyer Forsting et al.* [15] and *Strickland et al.* [8] In our LES, we also have to be careful when interpreting the results. In order to really quantify the power gain or loss of the solitary row, it is necessary to simulate for a longer period of time to reach a well-converged state, not only on the mean but also on the turbulent part. However, this is beyond the scope of this study.

5. Conclusions

In the framework of this study, we analysed the impact of a real wind farm cluster on the atmospheric boundary layer. We determined that global blockage is present for every conventionally neutral boundary layer. The dependency is strongly related to the combination of the strength of the temperature inversion and ABL height. Global blockage is particularly pronounced when a low ABL height is accompanied by a strong temperature inversion. Increasing the ABL height reduces the impact of temperature inversion strength on global blockage.

To quantify the loss of power produced by the first row, we also compared the case of which global blockage is most dominant with a solitary row and single turbine. This exhibits mainly that in our LES the front row of a wind farm cluster is being subjected to a loss of power. Differences in power production between single turbines and solitary rows have been observed. Longer simulations are required to reach a fully converged state in order to draw definitive conclusions.

This study serves as a basis for future work, in which the LES cases are being compared with a LiDAR measurement campaign, that measured the upstream and downstream wind velocity components of the Kaskasi gap, and in front of the northern most wind farm. Additional case studies should be added where a greater range of atmospheric conditions are being modelled, to capture a more accurate behaviour of the wind farm cluster on the ABL.

Acknowledgements

This work is partly funded by the Federal Ministry for Economic Affairs and Climate Action according to a resolution by the German Federal Parliament (project C2-wakes, grant no. 03EE3087B) and (project MOUSE, grant no. 03EE3067A). The authors gratefully acknowledge the computing time granted by the Resource Allocation Board and provided on the supercomputer Lise and Emmy at NHR@ZIB and NHR@Göttingen as part of the NHR infrastructure. The calculations for this research were conducted with computing resources under the projects nik00066 and nik00084. Also, some of the simulations were performed using the HPC Cluster MOUSE of the Carl von Ossietzky Universität Oldenburg (Germany) funded by the German Ministry of Economic Affairs and Climate Action (BMWK, grant no. 03EE3067A). Martin Kühn is acknowledged for his fruitful discussion and support.

References

[1] Bleeg J, Purcell M, Ruisi, R, & Traiger E. (2018). Energies 11(6) 1609
[2] Allaerts, D., & Meyers, J. (2017). J. Fluid Mech., 814, 95-130.

[3] Abkar, M., & Porté-Agel, F. (2013). Energies, 6(5), 2338-2361.
[4] Wu, K. L., & Porté-Agel, F. (2017). Energies, 10(12), 2164.
[5] Schneemann, J., Theuer, F., Rott, A., Dörenkämper, M., & Kühn, M. (2020). Wind Energy Sci., 1-26.
[6] Maas, O., & Raasch, S. (2022). Wind Energy Sci., 7(2), 715-739.
[7] Cañadillas, B., Foreman, R., Steinfeld, G., & Robinson, N. (2023). *Energies*, *16*(7), 2949.
[8] Strickland, J. M., & Stevens, R. J. (2022). Eur. J. Mech. B Fluids, 95, 303-314.
[9] Maronga B et al. (2020), GMD, 13(3), 1335-1372.
[10] Steinfeld, G.; Witha, B.; Dörenkämper, M.; Gryschka, Promet-Meteorol. Fortbild. 2016, 39, 163–180.
[11] Maas, O. (2022). Wind Energy Sci. Discussions, 2022, 1-31.
[12] Sanchez Gomez et al. (2023) Wind Energy Sci. Discussions, *2023*, 1-28.
[13] Smith, R. B. (2010). Wind Energy, 13(5), 449-458.
[14] Lanzilao, L., & Meyers, J. (2023). J. Fluid Mech., 979: A54.
[15] Meyer Forsting, A. R., Troldborg, N., & Gaunaa, M. (2017). Wind. Energy, 20(1), 63-77.
[16] Bleeg, J., & Montavon, C. (2022). *J. Phys. Conf. Ser.* Vol. 2265, No. 2.